doi:10.1016/j.jmb.2006.01.040 J. Mol. Biol. (2006) 357, 1253–1262

JMB

Available online at www.sciencedirect.com

SCIENCE DIRECT®

ELSEVIER

Conformational and Quantitative Characterization of Oritavancin–Peptidoglycan Complexes in Whole Cells of *Staphylococcus aureus* by *in Vivo* ^{13}C and ^{15}N Labeling

Lynette Cegelski[1], Dirk Steuber[1], Anil K. Mehta[1], Daniel W. Kulp[2] Paul H. Axelsen[2] and Jacob Schaefer[1]*

[1]*Department of Chemistry Washington University, St. Louis, MO 63130, USA*

[2]*Departments of Pharmacology Biochemistry and Biophysics and Medicine/Infectious Diseases, University of Pennsylvania School of Medicine, Philadelphia, PA 19104, USA*

**Corresponding author*

Solid-state NMR has been used to examine the cell walls of intact whole cells of *Staphyloccus aureus* grown on media containing D-[1-^{13}C]alanine, [^{15}N]glycine, and the alanine racemase inhibitor, alaphosphin. The results of *in situ* site-selective, four-frequency NMR experiments show directly for the first time that (i) 54% of the cell-wall peptidoglycan stems have D-alanine termini and 46%, D-alanine-D-alanine termini; (ii) the molar ratio of stems ending in D-alanine to esterified alditol repeats of cell-wall teichoic and lipoteichoic acids is 3:2; and (iii) 50% of the mature cell-wall binding sites for a fluorinated oritavancin analogue consist of two nearest-neighbor peptide stems of different glycan strands. The drug is bound to the D-Ala-D-Ala terminus of one stem and is proximate to the bridging pentaglycyl segment that cross-links the two stems. Structural details of the binding site are revealed in a model of the glycopeptide–peptidoglycan interaction produced by molecular dynamics simulations with internuclear distance restraints determined by NMR.

Keywords: dipolar coupling; glycopeptide antibiotic; magic-angle spinning; solid-state NMR; transglycosylase

Introduction

Vancomycin and other closely related glycopeptide agents (Figure 1), inhibit the biosynthesis of the peptidoglycan of the bacterial cell wall.[1] Cell-wall and septal thinning result from vancomycin treatment[2] because the balance between new cell-wall synthesis at the cell-membrane surface and enzymatic degradation of outer layers that normally functions to accommodate cell growth and division is dramatically perturbed. The antibiotics do not penetrate into the cytoplasm of the cell but form complexes with the D-Ala-D-Ala carboxyl termini of peptidoglycan precursors outside the cell membrane,[3,4] presumably including *N*-acetylglucosamine-*N*-acetyl-muramyl-pentapeptide-pyrophosphoryl-undecaprenol (lipid II). In principle, binding of vancomycin to lipid II could interfere with transglycosylase activity,[5,6] and possibly transpeptidase activity as well.[7] Both are essential for the synthesis of new cell wall. The former extends the glycan chain and the latter cross-links the peptide stems with the subsequent elimination of the terminal D-Ala (see Figure 2). Solid-state NMR measurements have been used to measure the production of cross-links and bridge-links in the cell walls of actively dividing *Staphylococcus aureus*. These experiments showed that transglycosylation is inhibited by vancomycin before any effect on transpeptidation is observed.[8]

For many years vancomycin was only used as a last resort because of its toxicity and the relatively high costs associated with its adminstration. When used, however, it was consistently effective.[7,9,10]

Abbreviations used: CPMAS, cross-polarization magic-angle spinning; lipid II, *N*-acetylglucosamine-*N*-acetyl-muramyl-pentapeptide-pyrophosphoryl-undecaprenol; REDOR, rotational-echo double resonance; TEDOR, transferred-echo double resonance; VRE, vancomycin-resistant enterococci; VRSA, vancomycin-resistant *S. aureus*.

E-mail address of the corresponding author: jschaefer@wustl.edu

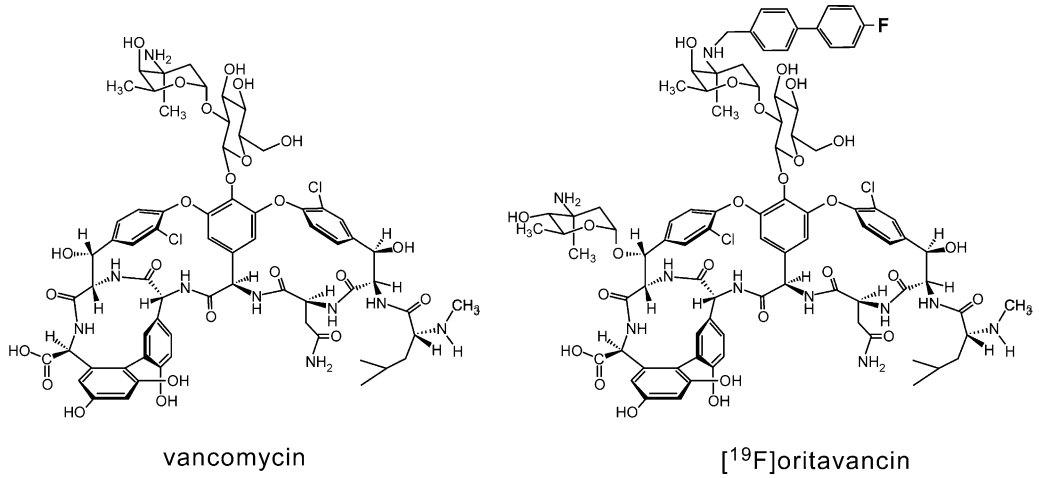

Figure 1. Chemical structures of vancomycin (left) and [^{19}F]oritavancin (right), Eli Lilly compound LY329332.

This began to change with the emergence of vancomycin-resistant enterococci and staphylococci. Vancomycin-resistant enterococci (VRE) appeared around 1988.[11] The first clinical isolate of *S. aureus* with reduced susceptibility to vancomycin (minimum inhibitory concentration, MIC, equal to 8 μg/ml) was identified in Japan in 1996;[12] full resistance corresponds to an MIC of at least 32 μg/ml. In 2002, vancomysin-resistant *S. aureus* (VRSA) with MIC > 128 μg/ml was recovered from a patient in Michigan who was being treated with multiple courses of antibiotics.[13] Vancomycin-resistant *Enterococcus faecalis* was also recovered from the patient. The VRSA isolate contained the *vanA* vancomycin-resistance gene from enterococci, probably through conjugative transfer from the

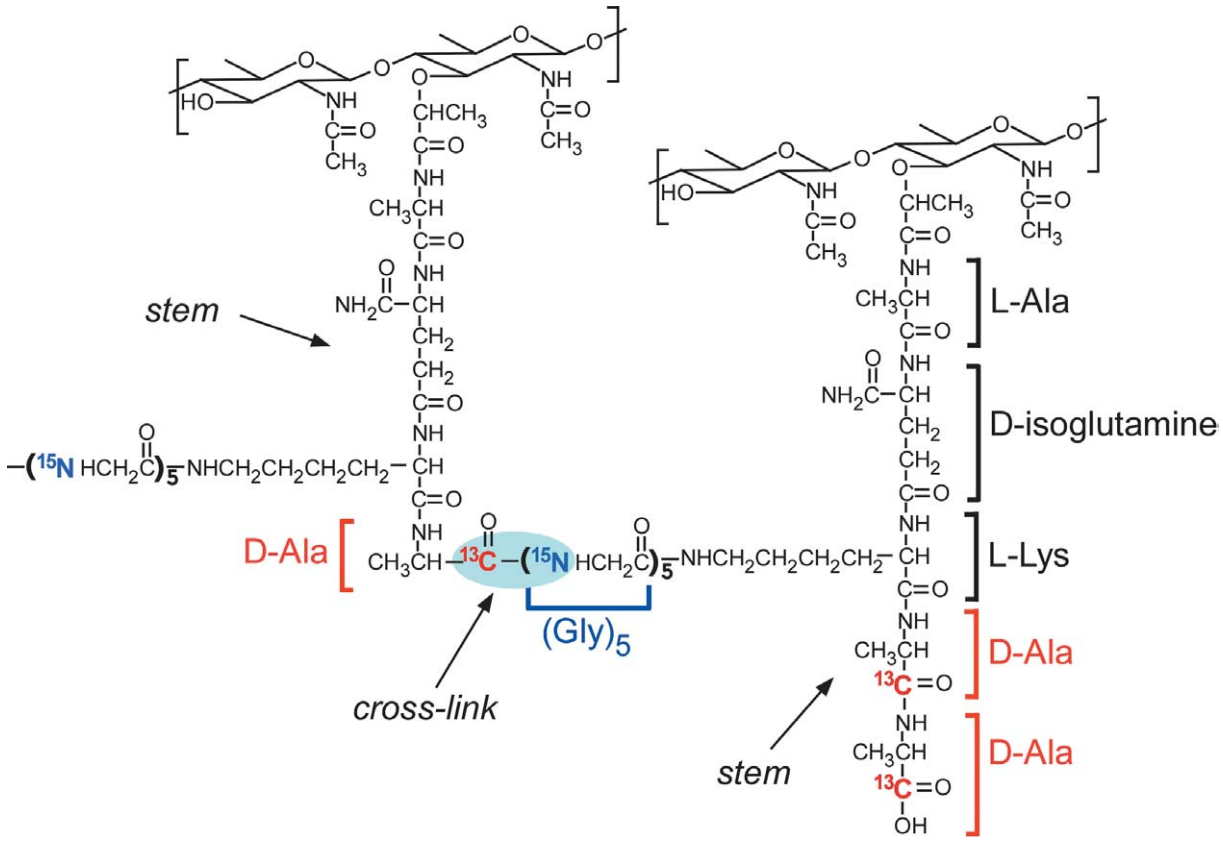

Figure 2. Chemical structures of two peptidoglycan stems in the cell walls of *S. aureus* grown on media containing D-[1-^{13}C]alanine, [^{15}N]glycine, and an alanine racemase inhibitor. The stem on the left contains a D-Ala-Gly1 cross-link site (light blue highlight). The bridging pentaglycyl segment is attached by Gly5 to the stem on the right, which ends in a D-Ala-D-Ala oritavancin binding site.

VRE isolate, as is possible *in vitro*.[14] In 2002 and 2004, two other VRSA clinical isolates were documented in New York.[15]

The seemingly inevitable emergence of resistance to almost any antibiotic underscores the need to understand the molecular details of specific modes of action to guide the development of potent, new antibiotics and to permit the rational implementation of combination antimicrobial therapies. Rotational-echo double resonance (REDOR) solid-state NMR is a structural biology tool that permits the atomic-level dissection of drug-bound whole-cell complexes. With REDOR, quantitative distance and orientation determinations can be made between drug and cell-wall nuclei. We recently used REDOR heteronuclear recoupling techniques to measure several distances from [^{19}F]oritavancin, Eli Lilly compound LY329332 (Figure 1), and ^{13}C, ^{15}N, and ^{2}H labels incorporated in the cell walls of *S. aureus*.[16,17] Oritavancin is a new semi-synthetic vancomycin analogue that exhibits increased efficacy against VRE.[18] The drug was complexed to both isolated cell walls and the cell walls of intact late log-phase whole cells. Results from the REDOR experiments demonstrated that when complexed with mature cells, [^{19}F]oritavancin does not form dimers. A crude model of the binding site consistent with the REDOR results, binding-assay results, and cell-wall compositional analysis, positioned vancomycin at the D-Ala-D-Ala terminus of a peptide stem with the fluorobiphenyl moiety of the antibiotic near the base of a second, cross-linked stem in a locally ordered peptidoglycan matrix.[16]

A complication for the quantitative use of whole-cell REDOR is that the exogenous labeled amino acids are incorporated into both cell walls and cytoplasmic proteins. The signals from labels in cytoplasmic proteins make the general determination of S_0 (the signal observed without rotor-synchronized dephasing pulses) for the cell wall impossible. Without the appropriate S_0, distance distributions of isolated spin pairs cannot be extracted reliably from REDOR dephasing.[17] Structural analysis requires the use of supplementary information, typically the compositional analysis of the cell wall.[16]

However, for whole cells of *S. aureus* labeled by D-[1-^{13}C]alanine and [^{15}N]glycine, grown in the presence of alaphosphin, a racemase inhibitor, ^{13}C labels are incorporated only in the cell wall, either in the D-Ala-D-Ala and D-Ala termini of peptidoglycan stems, or in the ester groups of teichoic acids.[19] In addition, the covalent ^{13}C links to ^{15}N labels (Figure 2) can be selectively detected by one-bond ^{15}N→^{13}C transferred-echo double-resonance (TEDOR) transfers.[20] Thus, D-[1-^{13}C]alanine and [^{15}N]glycine labeling combined with TEDOR detection provides information specific for cell-wall cross-links in whole cells of *S. aureus*.

Here, we report the results of experiments that exploit selectivity in both the labeling strategy and the NMR recoupling methods. Only whole-cell measurements are made and the TEDOR experiment eliminates the need for assumptions about cell-wall composition and isotopic enrichments of alanine residues in peptidoglycan stems and teichoic acid. The combination of TEDOR and REDOR measurements are employed to: (i) extract quantitative information about the cell-wall composition of *S. aureus*; (ii) measure the regularity of the oritavancin binding site in the cell wall; and (iii) provide accurate distance restraints for a molecular model of the binding site in intact whole cells. This is the first report of the application of combined TEDOR–REDOR to whole cells. The results highlight the ability of solid-state NMR to obtain unambiguous atomic-level structural information from a complex biological system. This strategy is not restricted to *S. aureus* and may be adapted to investigate the structure and mode of action of other antibiotics developed to combat antibiotic-resistant bacteria with altered cell-wall structures such as the D-Ala-D-Lac motif exhibited by VRE.

Results and Discussion

D-Alanine in the cell wall

The cross-polarization magic-angle spinning ^{13}C NMR spectrum of [^{19}F]oritavancin complexed with *S. aureus* whole cells (Figure 3, bottom) grown in media containing D-[1-^{13}C]Ala and [^{15}N]Gly, in the presence of alaphosphin, is dominated by the carbonyl-carbon peak centered at 175 ppm, which

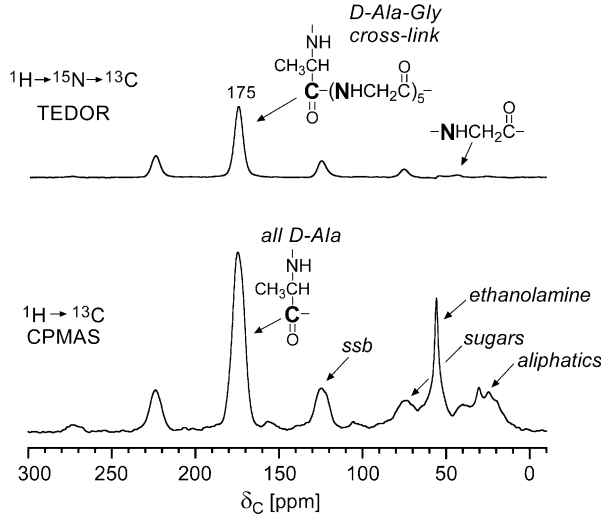

Figure 3. (Bottom) Cross-polarization magic-angle spinning (CPMAS) ^{13}C NMR spectrum of lyophilized whole cells of *S. aureus* grown on media containing D-[1-^{13}C]alanine, [^{15}N]glycine, and an alanine racemase inhibitor. The spectrum resulted from the accumulation of 256 scans. (Top) Transferred-echo double-resonance (TEDOR) ^{13}C NMR spectrum of the same whole-cell sample. The observed signals arise only from label and natural-abundance ^{13}C that is covalently bonded to ^{15}N. The spectrum resulted from the accumulation of 120,000 scans.

is due primarily to incorporation of labeled D-alanine into cell walls. The D-Ala appears in the termini of peptidoglycan stems (Figure 2), and also in alanyl ester side-chains of teichoic acid and lipoteichoic acid. Teichoic acids are polymers of alternating phosphate and alditol groups,[19] which are either covalently connected to the ends of peptidoglycan chains (wall teichoic acids), or to membrane glycolipids (lipoteichoic acids). They are highly charged and influence binding to the cell wall and enzyme activity within the cell wall.

The remaining peaks in the spectrum arise from natural-abundance carbon atoms in cytoplasm and cell walls. The $^{15}N \rightarrow {}^{13}C$ TEDOR spectrum is considerably simpler and is primarily just a single carbonyl-carbon peak and its spinning side bands (Figure 3, top). This TEDOR peak intensity has been scaled to take into account the experimental efficiency of the ^{15}N to ^{13}C transfer (40%, compared to the theoretical[20] 50%) and the ^{15}N isotopic enrichment of the glycine residues in the cell wall (65%, from a separate REDOR determination[21]). The isotopic concentration of ^{15}N bonded to D-[1-^{13}C]Ala (in D-Ala-D-Ala sequences) is 0.3%, so that the transfered *S* from that source is 100 times less than the observed TEDOR signal, which is more than 30% of the total intensity arising from labeled D-Ala (Figure 3). The intensity of the 175 ppm peak from natural-abundance ^{13}C-labeled whole cells[21] is about the same as the aliphatic-carbon signal intensity at 25 ppm (Figure 3, bottom), or about one-fifth of the signal intensity arising from all labeled D-Ala. This means that the transferred *S* from natural-abundance ^{15}N next to natural-abundance ^{13}C (all sources in the cell) is 500 times less than the observed TEDOR signal of Figure 3. Thus, the TEDOR peak is specific for cross-link sites in the cell walls.

The full linewidth of the TEDOR peak is about 6 ppm, considerably broader than observed for fully hydrated whole cells.[21] This comparison indicates conformational flexibility and spatial averaging for hydrated peptidoglycan stems and attached pentaglycyl segments. The lyophilization of the whole cell therefore traps a distribution of local orientations resulting in broad lines.

The CPMAS ^{13}C NMR spectrum of Figure 3 (bottom) has contributions from four types of carbonyl carbon atoms: (i) the peptide carbonyl in cross-linked stems ending in D-Ala whose signal appears at 175 ppm; (ii) the peptide carbonyl of D-Ala4 of D-Ala-D-Ala stems whose signal also appears at 175 ppm; (iii) the D-Ala5 terminal carboxyl of those stems at 177 ppm; and (iv) various teichoic acid D-Ala esters at 171 ppm.[22,23] This complicated spectrum can be experimentally deconvoluted because the 175 ppm cross-link contribution is determined directly by the TEDOR transfer (Figure 3, top) and is totally removed from the CPMAS spectrum by subtraction (Figure 4, second from bottom). In addition, the TEDOR peak provides a good model for the shift and lineshape of the 175 ppm peptide component of stems ending in

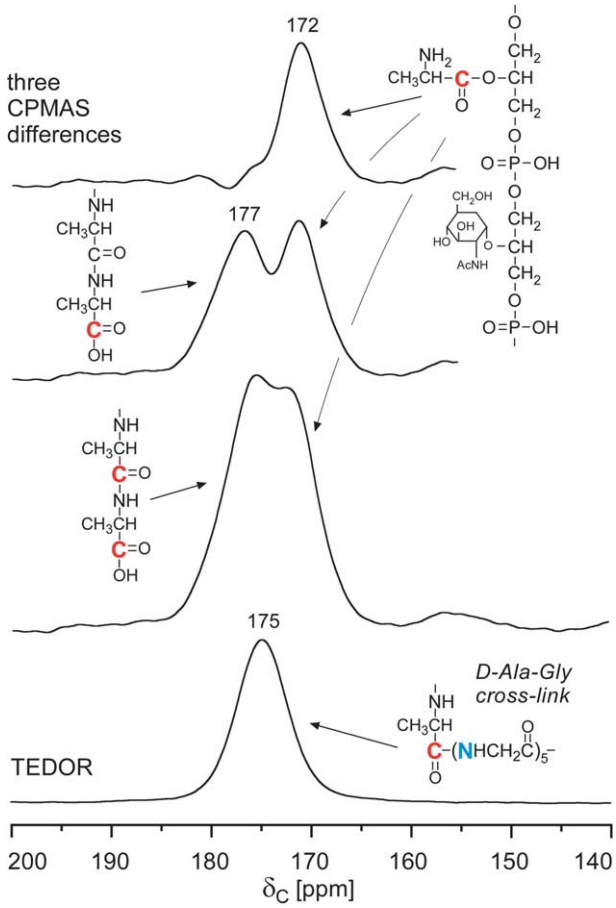

Figure 4. (Bottom) The TEDOR spectrum of Figure 3 on an expanded scale. (Second from bottom) The difference spectrum resulting from subtracting the TEDOR spectrum of Figure 3 from the CPMAS spectrum of Figure 3. (Second from top) The difference spectrum resulting from subtracting 1.86 times the TEDOR spectrum of Figure 3 from the CPMAS spectrum of Figure 3. (Top) The difference spectrum resulting from subtracting 0.86 times the TEDOR spectrum of Figure 3 from the second CPMAS difference spectrum (second from top), after shifting the TEDOR peak from 175 ppm to 177 ppm.

D-Ala-D-Ala, and, after a 2 ppm frequency shift to low field, for the shift and lineshape of the 177 ppm carboxyl component of the same stems. The carboxyl and peptide components of the D-Ala-D-Ala stems must have the same relative intensity. The absolute intensity of the D-Ala-D-Ala pair is determined by requiring that there is no residual intensity in the 177 ppm carboxyl-carbon region after the second subtraction of the 175 ppm TEDOR peak from the CPMAS spectrum (Figure 4, second from top), together with subtraction of the 177 ppm frequency-shifted TEDOR peak (Figure 4, top). Thus, the full deconvolution depends on only one fitting parameter: the scaling of the equal intensities of the D-Ala-D-Ala pair of peaks relative to the total spectrum.

The difference spectrum of Figure 4 (top) is optimized (that is, no negative going components) if the first and second 175 ppm TEDOR subtractions

differ by 0.86(±0.02). This scaling factor sets the concentration of D-Ala-D-Ala stems at 86% of the concentration of D-Ala stems, which corresponds to 46% of all peptidoglycan stems ending in D-Ala-D-Ala (0.86/1.86=0.46) and 54% ending in D-Ala. This is the first direct *in situ* measurement of the extent of cross-linking in a *S. aureus* cell wall. The 46% value for stems ending in D-Ala-D-Ala (as opposed to earlier cell-wall composition estimates of 50%) is in better agreement with solid-state ^{15}N NMR estimates[16] of the number of non-bridging (10–20%) and missing pentaglycyl segments (15%), the sum of which must match the number of stems that are not cross-linked.

Comparisons of the relative intensities of the top difference spectrum to the bottom TEDOR spectrum leads to the conclusion that the ratio of stems ending in D-Ala relative to the number of teichoic and lipoteichoic acid repeat units with alanyl ester groups is 1.6. This is the first direct *in situ* measurement of the extent of esterification of teichoic acids in *S. aureus*. The high level of D-Ala esters in teichoic acids indicates that the autolysins in the cell wall, which bind to teichoic acids through ionic interactions and which are responsible for cell-wall degradation, were fully active[24] at the time of [^{19}F]oritavancin complex formation.

TEDOR–REDOR

$^{1}H \rightarrow {}^{15}N \rightarrow {}^{13}C\{^{19}F\}$ whole-cell measurements define distances from the fluorine label of [^{19}F]oritavancin to the cross-link D-[1-^{13}C]Ala carbonyl carbon with no interferences from the natural-abundance background or from cytoplasmic labels. The experiment begins with a matched spin-lock transfer from protons to ^{15}N for high sensitivity. Next is a coherence transfer from ^{15}N to ^{13}C that is tailored to a 1.5 Å distance and so is specific for covalently labeled bonds.[20] The transfer results in an edited or selected spectrum containing only a resonance from cross-link sites. Pentapeptide stems that are not cross-linked do not contain a ^{13}C–^{15}N pair and do not contribute. The TEDOR spectrum is the S_0 spectrum for a subsequent REDOR measurement with dephasing by ^{19}F to measure the ^{13}C–^{19}F dipolar coupling. All background interferences are gone.[22,25]

The TEDOR–REDOR selectivity is illustrated in Figure 5. The ^{13}C 96-rotor cycle TEDOR-echo spectrum (Figure 5, left) arises from only ^{13}C-labeled D-alanine residues adjacent to an ^{15}N-labeled glycine. The small peak at 42 ppm is due to natural-abundance glycyl α-carbon atoms which are also selected by covalent ^{15}N contact. The 96-rotor cycle $^{13}C\{^{19}F\}$ $\Delta S/S_0$ measures the extent of contact between the cross-linked D-[1-^{13}C]alanine label and the [^{19}F]oritavancin label during 15.36 ms of dipolar evolution. The REDOR difference after 128 rotor cycles (20.48 ms) is about the same as after 96 rotor cycles, but the S_0 signal has decreased so that $\Delta S/S_0$ has increased (Figure 5, right). The diminution of the TEDOR-echo signal is due to homogeneous decay.

Drug–cell wall distances from REDOR dephasing

The dependence of $^{15}N \rightarrow {}^{13}C\{^{19}F\}$ dephasing on evolution time for *S. aureus* whole cells labeled by D-[1-^{13}C]alanine and [^{15}N]glycine and complexed by [^{19}F]oritavancin is shown in Figure 6. The dephasing fits best to a Gaussian distribution of distances (Figure 6, inset) with an average value

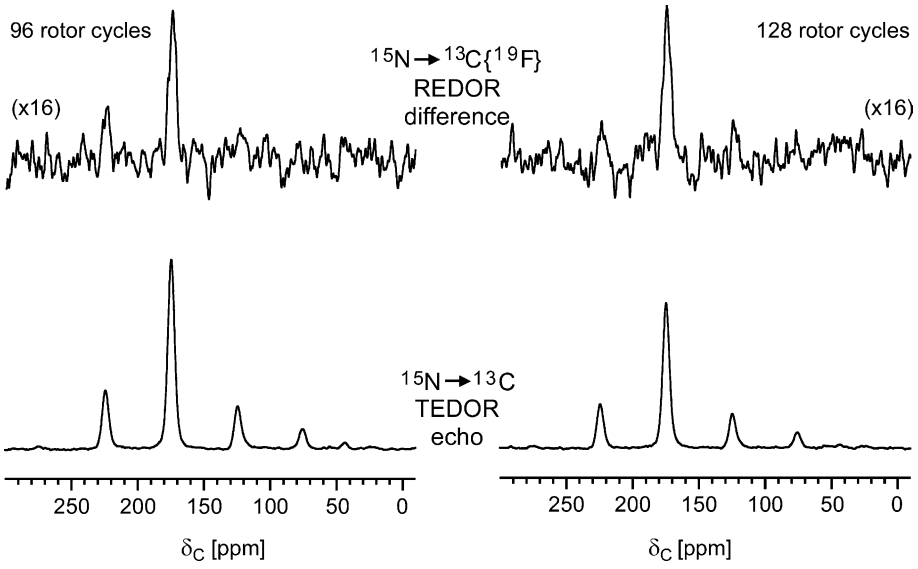

Figure 5. $^{15}N \rightarrow {}^{13}C\{^{19}F\}$ TEDOR-selected rotational-echo double-resonance (REDOR) spectra of the whole-cell sample of Figure 3 after dipolar evolution for (left) 96 rotor cycles and (right) 128 rotor cycles. TEDOR full echoes (S_0) are shown at the bottom of the Figure and the REDOR differences ($S_0 - S$, where S is the intensity of the dephased echo) at the top of the Figure. Each spectrum resulted from the accumulation of 120,000 scans. Magic-angle spinning was at 6250 Hz.

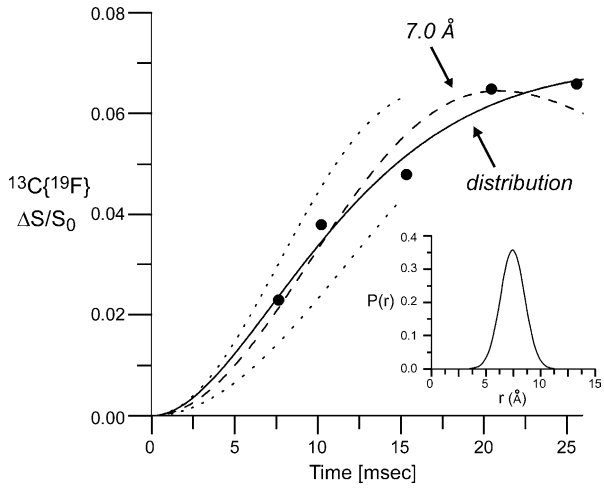

Figure 6. $^{15}N \rightarrow {}^{13}C\{^{19}F\}$ TEDOR-selected rotational-echo double-resonance (REDOR) integrated dephasing ($\Delta S/S_0$) of the whole-cell sample of Figure 3 as a function of dipolar evolution time. The estimated error is within the size of the filled symbols. The calculated dephasing for a 7 Å single distance from the fluorine of [^{19}F]oritavancin to the ^{13}C-labeled carbonyl carbon of the cross-link site (broken line) does not match the experimental dephasing as well as that calculated using a Gaussian distribution of distances centered at 7.4 Å (inset). The dotted lines show the calculated dephasing for single distances of 6.5 Å (upper) and 7.5 Å (lower).

of 7.4 Å and a full width of 1.6 Å. We consider the fitting to be qualitative and other distribution shapes would probably do as well. Each distance corresponds to an isolated ^{13}C–^{19}F pair at a single binding site, and the calculated dephasing is therefore a sum of independent contributions. A distribution in which all the distances are between 6 and 8 Å shows that the binding of [^{19}F]oritavancin is reasonably homogeneous, as suggested previously.[16] The earlier analysis, however, required several parameters that accounted for the statistics of labeled D- and L-alanine residues in the sample (which was prepared without inhibition of alanine racemization), as well as estimates of the relative numbers of cross-linked and free peptidoglycan stems. The present analysis of the TEDOR–REDOR measurement yields an absolute distance determination with no assumptions required.

Molecular model of the binding site

A model of the binding site resulting from the molecular dynamics simulations is shown in Figure 7. This model is consistent with all available REDOR data for [^{19}F]oritavancin bound to the mature cell wall of *S. aureus*.[16,17] The binding site (summarized in Tables 1–3) consists of two peptioglycan stems (purple) from different glycan strands (only terminal sugars shown in light green), connected covalently to one another by a bridging

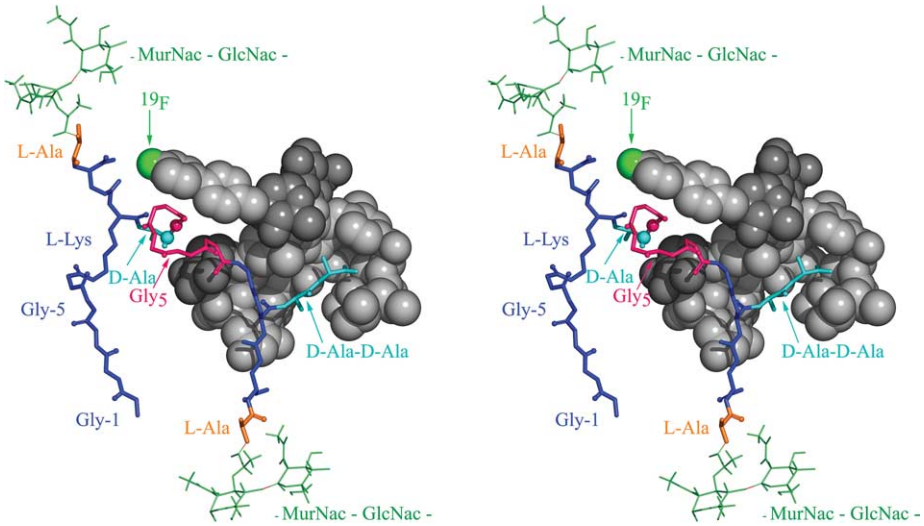

Figure 7. Molecular model of the binding of [^{19}F]oritavancin in the mature cell walls of *S. aureus*.

Table 1. [^{19}F]Oritavancin to peptidoglycan D-Ala-D-Ala binding site hydrogen-bond distance restraints for molecular dynamics simulations

Oritavancin N or O atom	Peptidoglycan C, N, or O atom	Lower bound (Å)	Upper bound (Å)	Final (Å)
2: HN	C (COO^- of D-Ala2)	1.8	3.6	2.9
3: HN	C (COO^- of D-Ala2)	1.8	3.6	3.0
4: HN	C (COO^- of D-Ala2)	1.8	3.6	3.0
4: O	HN (D-Ala1)	1.8	2.1	1.9
7: HN	O (L-Lys)	1.8	2.1	2.1

From Barna & Williams.[4]

Table 2. [^{19}F]Oritavancin to peptidoglycan stem and bridge distance restraints for molecular dynamics simulations

Oritavancin atom	Peptidoglycan C or N atom	Lower bound (Å)	Upper bound (Å)	Final (Å)
F	C=O (Gly5 in cross-linked bridge)[a]	10.9	∞	11.1
F	C=O (Gly1 in cross-linked bridge)[a]	4.9	5.1	5.2
F	N^{ζ} (L-Lys in cross-linked stem)[a]	11.0	∞	12.0
F	N^{ζ} (L-Lys in uncross-linked stem)[a]	11.0	∞	12.2
F	C=O (Gly1 in uncross-linked bridge)	13.3	∞	12.3
F	C=O (Gly5 in uncross-linked bridge)	13.3	∞	21.1
F	C^{α} (L-Ala)[b]	7.4	7.4	7.2
F	C=O (L-Ala)[b]	7.6	7.6	7.6
F	C^{β} (L-Ala)[b]	7.8	7.8	7.7
F	C=O (D-Ala cross-link site)[c]	7.4	7.4	7.5

[a] From Kim *et al.* [16]
[b] From Mehta *et al.* [17]
[c] From Figure 6 (inset).

pentaglycyl segment (red). The second pentaglycyl segment (purple) is not part of the binding site and is shown in an open conformation. The model in Figure 7 corresponds to the chemical structure shown in Figure 2. The [^{19}F]oritavancin is bound to the D-Ala-D-Ala end (light blue) of one of the stems with the fluorine label (green) proximate to the second, neighboring stem. The ^{19}F is: (i) 7.5 Å from the carbonyl-carbon ^{13}C (light blue) of the D-Ala-Gly1 cross-link that connects the two stems; (ii) at one end of the long axis of a compact bridging pentaglycyl segment (red); (iii) more than 10 Å from the connection of the bridge to the lysine of the bound stem (bridge-link at red-purple juntion); (iv) approximately 8 Å from the carbonyl carbon of L-Ala (gold) of the neighboring stem, with the α carbon a little closer than the carbonyl carbon and the methyl carbon a little farther.

Because adjacent stems detected in a TEDOR experiment must be cross-linked to one another, only one stem can be a binding site and antibiotic dimers will therefore not be present. This is consistent with the dephasing results of Figure 6, where the calculated dependence on evolution time and the asymptotic limit both indicate one ^{19}F dephasing center. Bound [^{19}F]oritavancin dimers require two adjacent stems each ending in D-Ala-D-Ala, an arrangement that would put two fluorine molecules near each bridging pentaglycyl segment.

Heterogeneity of cross-linking

The Gaussian distribution of distances used to fit the experimental $\Delta S/S_0$ predicts an asymptotic limit for the dephasing of 7.3% (Figure 6). This limit can be calculated from the fraction of all stems that end in D-Ala-D-Ala, and the fraction of these that are complexed by [^{19}F]oritavancin. The former is known from the TEDOR results of Figure 4 and the latter from the binding assay.[16] Pentaglycyl segments with a carbonyl ^{13}C label in each residue will dephase in a ^{13}C{^{19}F} experiment only if the segment is attached *via* Gly5 to a stem with [^{19}F]oritavancin bound to D-Ala-D-Ala. This is a consequence of the spatial proximities shown in Figure 7. A similar conclusion may be drawn when D-Ala residues each contain a ^{13}C carbonyl label and the glycyl residues each contain a ^{15}N label. A ^{15}N→^{13}C TEDOR transfer selects the cross-link site at D-Ala-Gly1, and the ^{13}C signal from this site will dephase in a ^{13}C{^{19}F} experiment only if the cross-link site is attached *via* Gly5 to a stem with [^{19}F]oritavancin bound to a D-Ala-D-Ala terminus. This latter situation is illustrated in Figure 2.

The TEDOR results of Figure 4 indicate that 54% of stems end in D-Ala and 46% in D-Ala-D-Ala. This means that 46% of stems neighboring a cross-link are binding sites, assuming that the distribution of binding sites throughout the cell wall is random. The binding assay showed that only 1/3 of all binding sites are occupied by [^{19}F]oritavancin (see Materials and Methods). Thus, the ^{13}C{^{19}F} asymptotic dephasing limit expected for the TEDOR-selected cross-link sites is (1/3)(0.46)=15%. The observed ^{15}N→^{13}C{^{19}F} limit, however, is only 7.3($\pm$0.3)% (Figure 6).

There are two possible explanations for this discrepency. One is heterogeneity in the conformation of bridging pentaglycyl segments such that half of them adopt a much different conformation from that illustrated in Figure 7. By this explanation, the distance from the cross-link site to the oritavancin fluorine would be outside the limits of detectability for 25 ms of dipolar evolution. This seems unlikely based on the homogeneous total (i.e. not TEDOR-selected) dephasing observed for ^{13}C-labeled stems and pentaglycyl segments.[16]

A more plausible explanation is heterogeneity in the distribution of cross-links in the mature cell wall resulting in more cross-links in the outer part of the mature cell wall, and more stems ending in D-Ala-D-Ala in the inner part. For two adjacent stems ending in D-Ala, both of the TEDOR-selected D-Ala-Gly1

Table 3. Pentaglycyl bridge distance restraints for molecular dynamics simulations

Stem atom	Bridge C atom	Lower bound (Å)	Upper bound (Å)	Final (Å)
N^{ζ} (L-Lys)	C=O (Gly1)	5.9	7.1	7.1

From Tong *et al.*[21]

cross-links contribute to S_0, and neither contributes to ΔS. This means that if the cross-links are not distributed randomly but are locally concentrated, the dephasing will be less than 15%. In fact, we can use the difference between the expected 15% and the observed 7% dephasing as a measure of the heterogeneity of the cross-link distribution. Thus, we conclude that the probability of finding adjacent pairs of stems ending in D-Ala is about twice the random-placement value.

Materials and Methods

Growth, labeling, and complexation of *S. aureus*

Cells of *S. aureus* (ATCC 6538P) were grown in a defined medium as described before[16] but in the presence of the alanine racemase inhibitor, alaphosphin (5 μg/ml). The cells were labeled by replacing an unlabeled amino acid of the medium by the corresponding labeled version. Cells were harvested at mid-log phase at an absorbance of 1.0 at 660 nm by centrifugation at 10,000*g* for 10 min at 4 °C, washed twice with 40 mM triethanolamine hydrochloride (pH 7.0), re-suspended in the same buffer, and complexed[16] with [^{19}F]oritavancin (3.75 mg LY329332 added to the equivalent of 140 mg cells, dry weight, corresponding to one-third occupancy of total binding sites). The suspension was frozen and lyophilized for NMR measurements.

Solid-state NMR

Spectra were obtained using a six-frequency transmission-line probe,[23] having a 12 mm long, 6 mm inside-diameter analytical coil and a Chemagnetics/Varian magic-angle spinning ceramic stator. Lyophilized samples were contained in thin-wall Chemagnetics/Varian 5 mm outside-diameter zirconia rotors. The rotors were spun at 6250 Hz with the speed under active control to within ±2 Hz. The spectrometer was controlled by a Tecmag Libra pulse programmer. Radiofrequency pulses for ^{13}C (126 MHz), and ^{15}N (50.3 MHz) were produced by 1 kW American Microwave Technology power amplifiers. Proton (500 MHz) and ^{19}F (470 MHz) radiofrequency pulses were generated by a 1 kW Amplifier Systems tube amplifier driven by a 50 W American Microwave Technology power amplifier. The π-pulse lengths were 5 μs for ^{19}F, 8 μs for ^{13}C, and 9 μs for ^{15}N. A 12-T static magnetic field was provided by an 89 mm bore Magnex superconducting solenoid. Proton–carbon cross-polarization magic-angle spinning (CPMAS) transfers were made with radiofrequency fields of 62.5 kHz. Proton dipolar decoupling was 100 kHz with TPPM modulation.[26]

REDOR was used to restore the dipolar couplings between heteronuclear pairs of spins that are removed by magic-angle spinning.[27] REDOR experiments are always done in two parts, once with rotor-synchronized dephasing pulses (S) and once without (full echo, S_0). The dephasing pulses change the sign of the heteronuclear dipolar coupling, and this interferes with the spatial averaging resulting from the motion of the rotor. The difference in signal intensity (REDOR difference, $\Delta S = S_0 - S$) for the observed spin in the two parts of the REDOR experiment is directly related to the corresponding distance to the dephasing spin.[27] All ^{13}C{^{19}F} REDOR spectra were collected with standard xy-8 phase cycling,[28] on both observed and dephasing channels, and with TPPM[26] of the proton decoupling during dipolar evolution. The xy-8 phase cycling resulted in experimental ^{13}C{^{19}F} dephasing that was within 4% of the expected value for an analytical standard after 15 ms of dipolar evolution and 128 π pulses.[29]

TEDOR from ^{15}N to ^{13}C was done by first creating bilinear ^{15}N–^{13}C coherence in four rotor cycles using ^{15}N{^{13}C} REDOR pulses, then transferring the coherence with simultaneous ^{13}C and ^{15}N π/2 pulses, and finally converting this coherence to observable ^{13}C magnetization with ^{13}C{^{15}N} REDOR pulses for an additional four rotor cycles.[20] The measured efficiency of the ^{15}N→^{13}C transfer on [1-^{13}C]MeA-[^{15}N]Val of a nine residue fragment of an emerimicin standard[25] was 40%. The full TEDOR–REDOR experiment added ^{13}C{^{19}F} dephasing pulses for ^{13}C magnetization selected by an ^{15}N→^{13}C TEDOR transfer.[22,25]

Molecular dynamics simulations

A model of the *S. aureus* peptidoglycan was created with CHARMm[30] by adaptation of version 27 polypeptide and polysaccharide topology files.[31] *N*-Acetyl-glucosamine and *N*-acetyl-muramic acid were derived from a glucose model and connected in alternating sequence *via* $\beta_{1\text{-}4}$ linkages to form four separate eight residue polysaccharide strands. The strands were all aligned parallel to the x axis, and positioned along the four parallel edges of a cube with dimensions $x = 55$ Å and $y = z = 110$ Å. The carboxylate group of each *N*-acetyl-muramic acid was linked *via* peptide bonds to the amino termini of L-Ala-D-Glu dipeptides. The γ-carboxylate group of each D-Glu was linked *via* peptide bonds to the amino termini of L-Lys-D-Ala-D-Ala tripeptides. The ε-amino group of each L-Lys residue was linked *via* peptide bonds to the carboxy termini of Gly_5 pentapeptides. The L-Ala-D-Glu-L-(Gly_5-Lys)-D-Ala-D-Ala segments attached to each polysaccharide strand were then oriented in a pattern that facilitated cross-link formation parallel to the y and z axes. One cross-link was formed between each pair of polysaccharide strands by deleting the C-terminal D-Ala residue, and joining the C terminus of the remaining D-Ala residue to the N terminus of a Gly_5 segment (Figure 2).

This model comprised a central image that was made infinite-periodic in three dimensions with two types of virtual bonds. One type of bond connected the last residue in each polysaccharide segment to the first residue by means of a virtual $\beta_{1\text{-}4}$ linkage. The second type involved deleting a C-terminal D-Ala residue, and joining the C terminus of the remaining D-Ala residue to the N terminus of a Gly_5 segment.

All polypeptide segments were originally created in extended conformation. Bonds and angles in the periodic system were regularized in CHARMm using several hundred cycles of steepest-descent and adapted-basis Newton-Raphson energy minimization with electrostatic terms off, and no solvent atoms present. Several chiral centers became incorrect during this procedure. These were corrected and the system was further minimized until stereochemical features remained correct during minimization. The central image dimensions following minimization were $x = 44.1$ Å and $y = z = 110$ Å.

A model of [^{19}F]oritavancin[32] was created within CHARMm by the addition of a fluorobiphenyl group to the model of chloroeremomycin described previously.[33] This model was placed within the peptidoglycan model,

and three sets of distance restraints were applied between the oritavancin and peptidoglycan models. One set (Table 1) mimicked the hydrogen bonds between the L-Lys-D-Ala-D-Ala residues and the oritavancin backbone (based on the known hydrogen bonding pattern in vancomycin–ligand complexes[4]). A second set (Table 2) represented the distances reported between the ^{19}F of oritavancin and various labeled positions in the peptidoglycan.[16,17] A third set (Table 3) consisted of a single restraint applied to create a compact pentaglycine bridge.[21] Following exhaustive energy minimization and 10 ps of room temperature *in vacuo* dynamics simulation, only minor restraint violations remained (Tables 1–3).

Acknowledgements

This paper is based on work supported by the National Institutes of Health under grant numbers AI43412 (to P.H.A.) and EB001064 (to J.S.).

References

1. Reynolds, P. E. & Somner, E. A. (1990). Comparison of the target sites and mechanisms of action of glycopeptide and lipoglycodepsipeptide antibiotics. *Drugs Exp. Clin. Res.* **16**, 385–389.
2. Molitor, E., Kluczny, C., Brotz, H., Bierbaum, G., Jack, R. & Sahl, H. G. (1996). Effects of the lantibiotic mersacidin on the morphology of staphylococci. *Zentralbl. Bakteriol.* **284**, 318–328.
3. Perkins, H. R. (1969). Specificity of combination between mucopeptide precursors and vancomycin or ristocetin. *Biochem. J.* **111**, 195–205.
4. Barna, J. C. & Williams, D. H. (1984). The structure and mode of action of glycopeptide antibiotics of the vancomycin group. *Annu. Rev. Microbiol.* **38**, 339–357.
5. Anderson, J. S., Matsuhashi, M., Haskin, M. A. & Strominger, J. L. (1967). Biosynthesis of the peptidoglycan of bacterial cell walls. II. Phospholipid carriers in the reaction sequence. *J. Biol. Chem.* **242**, 3180–3190.
6. Brotz, H., Bierbaum, G., Reynolds, P. E. & Sahl, H. G. (1997). The lantibiotic mersacidin inhibits peptidoglycan biosynthesis at the level of transglycosylation. *Eur. J. Biochem.* **246**, 193–199.
7. Reynolds, P. E. (1989). Structure, biochemistry and mechanism of action of glycopeptide antibiotics. *Eur. J. Clin. Microbiol. Infect. Dis.* **8**, 943–950.
8. Cegelski, L., Kim, J. S., Hing, A. W., Studelska, D. R., O'Connor, R. D., Mehta, A. K. & Schaefer, J. (2002). Rotational-echo double-resonance characterization of the effects of vancomycin on cell wall synthesis in *Staphylococcus aureus*. *Biochemistry*, **43**, 13053–13058.
9. Sapico, F. L., Montgomerie, J. Z., Canawati, H. N. & Aeilts, G. (1981). Methicillin-resistant *Staphylococcus aureus* bacteriuria. *Am. J. Med. Sci.* **281**, 101–109.
10. Sieradzki, K. & Tomasz, A. (1996). A highly vancomycinresistant laboratory mutant of Staphylococcus aureus. *FEMS Microbiol. Letters*, **142**, 161–166.
11. Johnson, A. P., Uttley, A. H. C., Woodford, N. & George, R. C. (1990). Resistance to vancomycin and teicoplanin: an emerging clinical problem. *Clin. Microbiol. Rev.* **3**, 280–291.
12. Hiramatsu, K., Aritaka, N., Hanaki, H., Kawasaki, S., Hosoda, Y., Hori, S. *et al*. (1997). Dissemination in Japanese hospitals of strains of *Staphylococcus aureus* heterogeneously resistant to vancomycin. *Lancet*, **350**, 1670–1673.
13. Centers for Disease Control and Prevention. (2002). *Staphylococcus aureus* resistant to vancomycin. *MMWR*, **51**, 565–567.
14. Noble, W. C., Virani, Z. & Cree, R. G. (1992). Co-transfer of vancomycin and other resistance genes from *Enterococcus faecalis* NCTC 12201 to *Staphylococcus aureus*. *FEMS Microbiol. Letters*, **72**, 195–198.
15. Centers for Disease Control and Prevention. (2002). Vancomycin-resistant *Staphylococcus aureus*. *MMWR*, **51**, 902.
16. Kim, S. J., Cegelski, L., Studelska, D. R., O'Connor, R. D., Mehta, A. K. & Schaefer, J. (2002). Rotational-echo double-resonance characterization of vancomycin binding sites in *Staphylococcus aureus*. *Biochemistry*, **41**, 6967–6977.
17. Mehta, A. K., Cegelski, L., O'Connor, R. D. & Schaefer, J. (2003). REDOR with a relative full-echo reference. *J. Magn. Reson.* **163**, 182–187.
18. Malabarba, A., Nicas, T. I. & Thompson, R. C. (1997). Structural modifications of glycopeptide antibiotics. *Med. Res. Rev.* **17**, 69–137.
19. Pooley, H. M. & Karamata, D. (1994). Teichoic acid synthesis in *Bacillus subtitis*: genetic organization and biological roles. In *Bacterial Cell Wall* (Ghuysen, J.-M. & Hakenbeck, R., eds), pp. 187–197, Elsevier Science, Amsterdam, Netherlands.
20. Hing, A. W., Vega, S. & Schaefer, J. (1992). Measurement of heteronuclear dipolar coupling by transferred-echo double-resonance NMR. *J. Magn. Reson.* **96**, 205–209.
21. Tong, G., Pan, Y., Dong, H., Pryor, R., Wilson, G. E. & Schaefer, J. (1997). Structure and dynamics of pentaglycyl bridges in the cell walls of *Staphylococcus aureus* by ^{13}C–^{15}N REDOR NMR. *Biochemistry*, **36**, 9859–9866.
22. McDowell, L. M., Schmidt, A., Cohen, E. R., Studelska, D. A. & Schaefer, J. (1996). Structural constraints on the ternary complex of 5-enolpyruvylshikimate-3-phosphate synthase from rotational-echo double-resonance NMR. *J. Mol. Biol.* **256**, 160–171.
23. Schaefer, J. & McKay, R. A. (1999). Multi-tuned single coil transmission line probe for nuclear magnetic resonance spectrometer. U.S. Patent 5,861,748.
24. Peschel, A., Vuong, C., Otto, M. & Götz, F. (2000). The D-alanine residues of *Staphylococcus aureus* teichoic acids alter the susceptibility to vancomycin and the activity of autolytic enzymes. *Antimicrob. Agents Chemother.* **44**, 2845–2847.
25. Holl, S. M., Marshall, G. R., Beusen, D. D., Kociolek, K., Redlinski, A. S., Leplawy, M. T. *et al*. (1992). Determination of an 8-Å interatomic distance in a helical peptide by solid-state NMR spectroscopy. *J. Am. Chem. Soc.* **114**, 4830–4833.
26. Bennett, A. E., Rienstra, C. M., Auger, M., Lakshmi, K. V. & Griffin, R. G. (1995). Heteronuclear decoupling in rotating solids. *J. Chem. Phys.* **103**, 6951–6958.
27. Gullion, T. & Schaefer, J. (1989). Detection of weak heteronuclear dipolar coupling by rotational-echo double-resonance nuclear magnetic resonance. *Advan. Magn. Reson.* **13**, 57–83.
28. Gullion, T., Baker, D. B. & Conradi, M. S. (1990). New, compensated Carr-Purcell sequences. *J. Magn. Reson.* **89**, 479–484.
29. Weldeghiorghis, T. K. & Schaefer, J. (2003). Compensating for pulse imperfections in REDOR. *J. Magn. Reson.* **165**, 230–236.
30. Brooks, B. R., Bruccoleri, R. E., Olafson, B. D., States, D. J., Swaminathan, S. & Karplus, M. (1983). CHARMm—a program for macromolecular energy,

minimization, and dynamics calculations. *J. Comp. Chem.* **4**, 187–217.
31. MacKerell, A. D., Bashford, D., Bellott, M., Dunbrack, R. L., Evanseck, J. D., Field, M. J. *et al*. (1998). All-atom empirical potential for molecular modeling and dynamics studies of proteins. *J. Phys. Chem. B*, **102**, 3586–3616.
32. Loll, P. J. & Axelsen, P. H. (2000). The structural biology of molecular recognition by vancomycin. *Annu. Rev. Biophys. Biophys. Struct.* **29**, 265–289.
33. Jusuf, S., Loll, P. J. & Axelsen, P. H. (2003). Configurational entropy and cooperativity between ligand binding and dimerization in glycopeptide antibiotics. *J. Am. Chem. Soc.* **125**, 3988–3994.

Edited by A. G. Palmer III

(Received 25 August 2005; received in revised form 24 December 2005; accepted 6 January 2006)
Available online 30 January 2006